The afterglow mystery of pulsed glow discharges and the role of dissociative electron–ion recombination†

Annemie Bogaerts

Received 19th December 2006, Accepted 19th March 2007
First published as an Advance Article on the web 12th April 2007
DOI: 10.1039/b618035c

It is generally recognized that excited level populations and, hence, optical emission intensities in pulsed glow discharges exhibit a peak upon pulse termination, *i.e.*, in the so-called afterglow. This afterpeak formation is attributed in many papers to electron–ion recombination, but up to now this hypothesis could not be confirmed quantitatively by numerical modelling, because of too low electron and ion number densities and recombination rate coefficients. In the present paper, we show the calculation results of a model, which includes also Ar_2^+ ions, beside the Ar^+ ions, and which takes into account the thermalization of the electrons upon pulse termination, yielding higher recombination rate coefficients. The role of electron–Ar_2^+ dissociative recombination and electron–Ar^+ three-body recombination as afterpeak formation mechanisms is investigated. Our study clearly shows the important role of Ar_2^+ ions and dissociative recombination in the afterpeak formation in the afterglow of pulsed discharges.

1. Introduction

Pulsed glow discharges have some distinct advantages compared with non-pulsed glow discharges.[1–3] Indeed, because the voltage and current are applied over short periods of time (of the order of milliseconds or microseconds), higher peak voltages and currents can be obtained for the same average power, resulting in enhanced sputtering, excitation and ionization, and therefore higher signal intensities.[4–7] The overall (time-averaged) sputter rates can, however, be kept low, opening up possibilities in the field of thin film analysis.[8,9] In addition, the glow discharge plasma passes through different temporal regimes, in which the excitation and ionization conditions change, and thus offers fast tunability for obtaining either atomic, molecular or structural information, thereby allowing fast speciation analysis.[10–15] Furthermore, because analyte and background species appear to be formed at different times in or after the pulse, background signals can be reduced, and hence better signal-to-background ratios can be obtained, when applying time-resolved detection.[16–21] By applying a second pulse during the time-window between the first applied voltage pulse and signal collection (the so-called double pulse configuration), the ion signals could be further increased provided that appropriate pulsing delays and gas flow rates were applied.[22]

The time-behaviour of pulsed glow discharges is, however, not yet fully understood. It is generally known that the signal intensities of optical emission lines exhibit a peak in the so-called afterglow, *i.e.*, when the voltage pulse is turned off. This is attributed in many papers[23–31] to electron–ion recombination, which populates the highest excited levels, followed by radiative decay to lower levels. However, this plausible explanation could not be verified quantitatively up to now, because the electron and Ar^+ ion densities calculated with numerical modelling, and the recombination rate coefficients adopted from the literature, appear to be too low to account for sufficient electron–ion recombination.[32–34] The latter process could only become sufficiently relevant if the electron population was assumed to rise by several orders of magnitude after pulse termination, due to thermalization,[34] but this assumption was in contradiction with recent experimental measurements.[35]

For this reason, it is necessary to look for other possible explanations. There exist several mechanisms for electron–Ar^+ ion recombination, *i.e.*:

- radiative recombination, in which the excess energy of recombination is carried away by a photon: $Ar^+ + e^- \rightarrow Ar^* + h\nu$;
- three-body recombination, in which the third body is an electron (also called collisional–radiative recombination): $Ar^+ + e^- + e^- \rightarrow Ar^* + e^-$;
- three-body recombination where the third body is another species (atom or molecule or the wall, this is also called neutral-stabilized recombination): $Ar^+ + e^- + X \rightarrow Ar^* + X$.

Three-body recombination with an electron as third body is recognized as the most important recombination mechanism,[34] but the rate was found to be still too low to account for sufficient recombination at the typical Ar^+ and electron densities to be expected in the afterglow.[34]

Another possibility is dissociative recombination with Ar_2^+ ions ($Ar_2^+ + e^- \rightarrow Ar^* + Ar$), which is characterized by a much higher rate coefficient (see below). In the present paper, we want to investigate the role of dissociative recombination in the production of highly excited states in the afterglow. For

Research Group PLASMANT, Department of Chemistry, University of Antwerp, Universiteitsplein 1, B-2610 Wilrijk-Antwerp, Belgium. E-mail: annemie.bogaerts@ua.ac.be

† The HTML version of this article has been enhanced with colour images.

this purpose, we have developed a model that describes not only the Ar^+ ions and electrons, but also the Ar_2^+ ions. The different production and loss mechanisms for these species, as well as some other details of the model, will be explained in Section 2. The results of the model, such as the temporal evolution of the species densities and of the various ionization and recombination rates upon pulse termination, will be presented in Section 3, and a discussion about the role of dissociative recombination in the afterpeak formation will be given in Section 4. Finally, Section 5 gives the conclusion.

2. Description of the model

The model is largely based on our models developed before for pulsed glow discharges,[32–34] but for the present investigation, we additionally describe the behaviour of the Ar_2^+ ions. We focus in this work on the formation of the afterpeak in excited level populations of Ar atoms. Hence, the species considered in the model include Ar ground state atoms, Ar atoms in several excited levels, fast Ar atoms in the cathode dark space (CDS), Ar^+ and Ar_2^+ ions, and electrons. Sputtered atoms and their corresponding ions are not incorporated here, because they have no major effect on the overall discharge behaviour,[36] and they increase the calculation time and complexity of the modelling network. In the following, we will give a brief overview of the modelling network, *i.e.*, which kind of model is used for which kind of species. We will not go into detail about the individual models considered here, because this information can largely be found back in our previous papers,[37–41] but we focus only on the new and most relevant aspects.

The Ar atoms are assumed to be thermal at the gas temperature measured recently in millisecond pulsed glow discharges,[35] and uniformly distributed throughout the discharge. The electrons are split up into an energetic group, treated with a Monte Carlo method,[37,38] and a thermal group, handled in a fluid model.[38] This fluid model also treats the Ar^+ and Ar_2^+ ions,[39] and it solves the species conservation and flux equations together with the Poisson equation, in order to obtain a self-consistent electric field distribution.[38] The Ar^+ ions are also described with a Monte Carlo model in the CDS,[37,40] because they can give rise to additional ionization if accelerated to sufficiently high energies. This Monte Carlo code also simulates the behaviour of the fast Ar atoms, formed in the CDS from the Ar^+ ions.[37,40]

The production and loss processes for the Ar^+ and Ar_2^+ ions, described in the fluid model, are summarized in Table 1. This gives also immediate information on the production and loss mechanisms of the electrons. The Ar^+ ions are formed by electron, fast Ar^+ ion and fast Ar atom impact ionization (reactions 1–3, respectively), which are treated in the corresponding Monte Carlo models (see above), based on cross sections as a function of energy.[37,40] Moreover, they can also be created by Ar metastable–metastable collisions (reaction 4), which are calculated from the Ar metastable atom densities in the collisional–radiative model described below, multiplied by the rate constant, adopted from ref. 42. Loss of the Ar^+ ions is considered to occur by three-body recombination with electrons (reaction 5), which was found to be the most important Ar^+–electron recombination process[34] (see also discussion above; hence the other recombination processes could be neglected). The rate constant varies strongly with electron temperature,[43] as indicated in Table 1 and illustrated in Fig. 1. This is an important fact, because it is generally recognized that the electrons undergo thermalization shortly after pulse termination, and hence the rate constant of electron–ion recombination can rise drastically. It is assumed that the Ar atoms are formed in highly excited states (denoted as Ar** in Table 1) by this recombination process. Conversion of Ar^+ ions into Ar_2^+ ions by collision with two Ar atoms (reaction 6) represents another loss mechanism for the Ar^+ ions, and the rate constant for this process was adopted from ref. 44. Besides the latter process, Ar_2^+ ions can also be formed by Ar metastable–metastable associative ionization (reaction 7), and by the so-called Hornbeck–Molnar associative ionization, resulting from collisions between highly excited Ar atoms and ground state atoms (reaction 8). It can be assumed that the latter process occurs for all Ar excited levels with energy above 14.43 eV, which is the bottom of the potential well for Ar_2^+ ions (*i.e.*, 15.76 eV (ionization energy of Ar) −1.33 eV (bond dissociation energy of Ar_2^+)). The densities of the Ar metastable atoms and of the higher excited Ar levels are calculated

Table 1 Overview of the production and loss processes of Ar^+ and Ar_2^+ ions, taken into account in the fluid model, as well as the values of the rate coefficients assumed, and references from where the data were adopted. These processes define the ionization–recombination balance in the pulsed glow discharge plasma. Note that Ar_m* and Ar** symbolize the Ar atoms excited to the (low-lying) metastable levels and to the highly excited levels, respectively

Production of Ar^+ ions		
(1) Electron impact ionization	$e^- + Ar^0 \rightarrow Ar^+ + 2\,e^-$	$\sigma(E)$ (electron MC model)
(2) Ar^+ ion imact ionization	$Ar^+ + Ar^0 \rightarrow Ar^+ + Ar^+ + e^-$	$\sigma(E)$ (Ar^+ ion MC model)
(3) Fast Ar^0 atom impact ionization	$Ar^0_f + Ar^0 \rightarrow Ar^+ + Ar^0_f + e^-$	$\sigma(E)$ (fast Ar atom MC model)
(4) Ar metastable–metastable ionization	$Ar_m^* + Ar_m^* \rightarrow Ar^+ + Ar^0 + e^-$	$k = 6.3 \times 10^{-10}$ cm^3 s^{-1} (ref. 42)
Loss of Ar^+ ions		
(5) Three-body electron–ion recombination	$Ar^+ + e^- + e^- \rightarrow Ar^{**} + e^-$	$k = 10^{-19}\,(T_e/300)^{-9/2}$ cm^6 s^{-1} (ref. 43)
(6) Ar^+ to Ar_2^+ ion conversion	$Ar^+ + 2\,Ar^0 \rightarrow Ar_2^+ + Ar^0$	$k = 2.7 \times 10^{-31}$ cm^6 s^{-1} (ref. 44)
Production of Ar_2^+ ions		
(6) Ar^+ to Ar_2^+ ion conversion	$Ar^+ + 2\,Ar^0 \rightarrow Ar_2^+ + Ar^0$	$k = 2.7 \times 10^{-31}$ cm^6 s^{-1} (ref. 44)
(7) Ar metastable–metastable associative ionization	$Ar_m^* + Ar_m^* \rightarrow Ar_2^+ + e^-$	$k = 5.7 \times 10^{-10}$ cm^3 s^{-1} (ref. 42)
(8) Hornbeck Molnar associative ionization	$Ar^{**} + Ar^0 \rightarrow Ar_2^+ + e^-$	$k = 2 \times 10^{-9}$ cm^3 s^{-1} (ref. 45)
Loss of Ar_2^+ ions		
(9) Electron–ion dissociative recombination	$Ar_2^+ + e^- \rightarrow Ar^{**} + Ar^0$	$k = 8.5 \times 10^{-7}\,(T_e/300)^{-0.67}\,(T_g/300)^{-0.58}$ cm^3 s^{-1} (refs. 46 and 47)

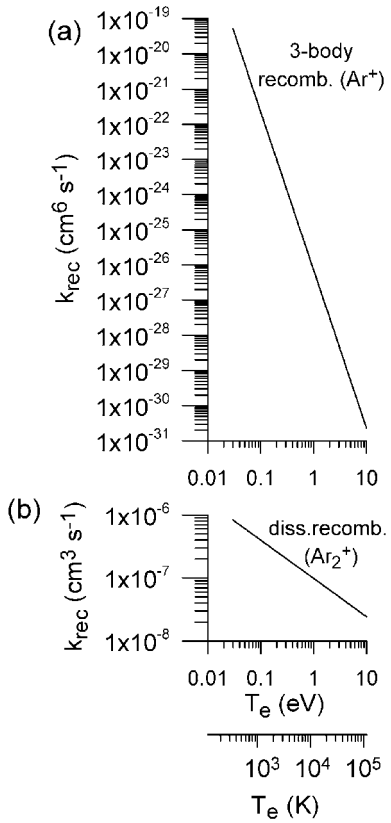

Fig. 1 Rate coefficients of electron–Ar^+ three-body recombination (a) and electron–Ar_2^+ dissociative recombination (b) as a function of electron temperature, calculated with the formulae presented in Table 1.

with the collisional–radiative model described below. The rate constants for both processes were adopted from refs. 42 and 45, respectively. Finally, loss of the Ar_2^+ ions is attributed to dissociative recombination (reaction 9). The rate constant of this process is much higher than for electron–Ar^+ ion recombination,[46,47] indicating that the process is much more effective, because the collision product can dissociate and the recombination energy can be converted into kinetic and potential energy of the dissociation products. The rate constant is, however, a much weaker function of the electron temperature than for three-body electron–Ar^+ ion recombination, as indicated in Table 1 and shown in Fig. 1.

Finally, the Ar atoms in excited levels are treated with a collisional–radiative model.[41] This model considers 64 different excited levels of Ar; some of them are individual levels (such as the four $3p^5$ 4s metastable and resonant levels), but most of the levels are lumped into effective levels, with a total statistical weight and an average excited energy. Fig. 2 illustrates the energy level scheme considered in the model, because it is relevant in the light of the discussion presented in the next section. However, it will not be explained in detail, because this information can be found back in ref. 41. For every (effective) level a balance equation with different production and loss processes is constructed. The production and loss mechanisms taken into account include electron, Ar^+ ion and Ar^0 atom impact excitation and de-excitation between all the levels, electron, Ar^+ ion and Ar^0 atom impact ionization from all levels, and radiative decay between all levels. For the highest excited levels included in the model, also three-body electron–ion recombination (of Ar^+ ions) and dissociative recombination (of Ar_2^+ ions) are taken into account. Finally, for the $3p^5$ 4s metastable levels some additional processes were incorporated, because they have a longer lifetime in the glow discharge plasma. These additional processes include metastable–metastable collisions, yielding either ionization of one of the atoms, or associative ionization with formation of Ar_2^+ ions (*cf.* above), as well as two-body and three-body collisions with Ar ground state atoms, yielding quenching of the metastable states. More details about this model, and the data for the production and loss processes of the various excited levels, can be found in ref. 41.

The models described above are coupled to each other due to the interaction processes between the different species, *i.e.*, the output of one model (*e.g.*, reaction rates) is used as input (source terms) in the other models. Hence, the different models need to be solved iteratively until final convergence is reached.

3. Results

The modelling network is applied to typical conditions of a millisecond pulsed glow discharge, as investigated by Gamez *et al.*,[35] in order to allow some comparison with the experimental data, such as for the electron number densities. The glow discharge cell was considered as a cylinder with 5 cm length and 5 cm diameter. The cathode is found at the top of the cylinder, with a diameter of 1.2 cm. The applied voltage as a function of time, and the resulting calculated electrical current (obtained from the microscopic fluxes of the charged species at the cathode), are plotted in Fig. 3. In order to obtain an electrical current in correspondence with the experiment,[35] a pressure of 0.7 Torr instead of 1 Torr had to be assumed, but this could be due to uncertainties in the reaction rate data, secondary electron emission yield at the cathode, *etc*. The gas temperature was assumed to be of the order of 450 K, in correspondence with the experiments.[35] It is worth mentioning that the experiments also revealed temporal and spatial changes in the gas temperature,[35] but these are not incorporated in our calculations because it would complicate the modelling network (and increase the calculation time) significantly, and we believe that they would not have a major effect on the calculation results. The voltage is applied for 5 ms, and then switched off. The calculated electrical current was found to be nearly constant during the entire pulse. Upon pulse termination, the current is predicted to drop to negligible values within about 0.5 ms.

Because we are focusing here on the afterpeak behaviour, results will only be presented from nearly the end of the pulse, where the plasma reaches steady-state conditions, until the densities have decayed to low values in the afterglow, more specifically from 4 to 6 ms.

(a) Densities of electrons, Ar^+ and Ar_2^+ ions

Fig. 4 illustrates the calculated densities of electrons, Ar^+ and Ar_2^+ ions, at the maximum of their spatial profiles (*cf.* Fig. 5 below), as a function of time around pulse termination. The

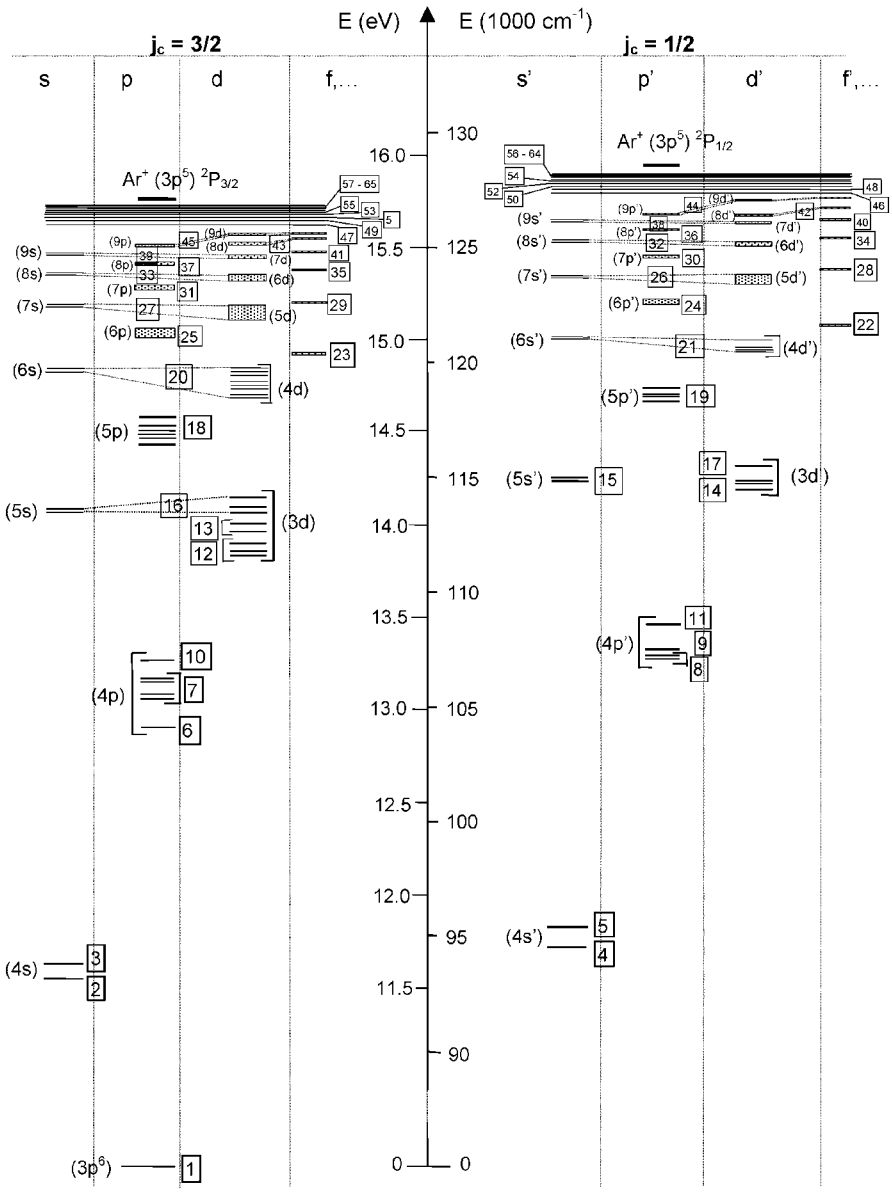

Fig. 2 Energy level scheme of the Ar excited levels, taken into account in the collisional–radiative model.[41] Most of the levels are lumped together into effective levels. The numbers indicated in rectangular boxes correspond to the effective level numbers in the model, and will be referred to later in this paper. More information about the levels can be found in ref. 41.

electron density is about 6×10^{11} cm^{-3} during the pulse and shows a little rise immediately after the voltage is turned off, for less than 40 μs, and then drops quickly to very low values after 1 ms. The initial rise can be attributed to a shift of the electron density towards the cathode, as a result of the changing potential distribution upon pulse termination, as will be illustrated below. The calculated absolute value of the electron density is in reasonable agreement with Thomson scattering experiments,[35] where values of 4×10^{11}–1.2×10^{12} cm^{-3} were obtained. Experimentally no rise in the electron density was observed, but the measurements report data at 4.9, 5.1 and 5.2 ms, whereas the model predicts this small rise only between 5.01 and 5.04 ms. At 5.1 ms, the calculated electron density has also dropped to 2.3×10^{11} cm^{-3}, hence about 38% of the plateau value, which is in good agreement with the experimental observations.

The Ar^+ ion density is calculated to be around 4.3×10^{11} cm^{-3} during the pulse, and it is also characterized by a small (and short) rise upon pulse termination (attributed to the changing potential distribution), followed by a pronounced drop to negligible values at 0.5–1 ms after pulse termination. The Ar_2^+ ions appear to have a density of 2.4×10^{11} cm^{-3} during the pulse, which is more than half of the Ar^+ ion density. Upon pulse termination, the Ar_2^+ ion density decays more slowly than the Ar^+ ions, so that after 0.1 ms, the Ar_2^+ and Ar^+ ion densities are comparable to each other. This slower drop is attributed to the fact that the Ar_2^+ ions can be populated by Hornbeck–Molnar associative ionization,

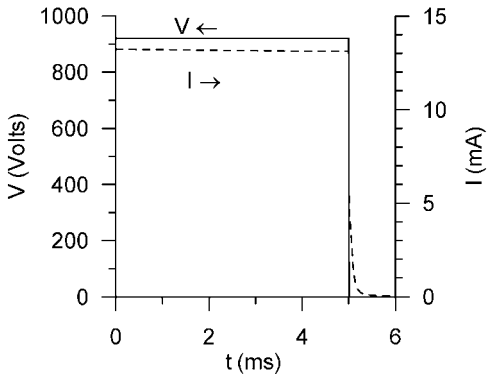

Fig. 3 Applied voltage (continuous line, left axis) and calculated electrical current (broken line, right axis) as a function of time, during and after the pulse.

associated with the highly excited Ar levels which exhibit a rise in population density upon pulse termination (see below).

The one-dimensional spatial density profiles of the electrons, Ar^+ and Ar_2^+ ions (*i.e.*, densities at the cell axis, as a function of distance from the cathode) are plotted in Fig. 5, at different times after pulse termination. The *y*-axes are plotted on the same scale, to visualize the differences in absolute values of the three species. Also shown is the potential distribution at the same time. During the pulse (*cf.* at 5 ms) the potential is −1000 V at the cathode, and drops quickly to zero at about 3.5 mm from the cathode, which is considered as the end of the CDS. In the negative glow (NG), the potential is nearly constant and around 33 V. The electron density is zero in the CDS, whereas the Ar^+ and Ar_2^+ ion densities reach low values in this region, resulting in a small positive space charge, which gives rise to the pronounced potential drop in the CDS. In the NG, the Ar^+ ion density is mainly concentrated in the first two centimetres, where electron impact ionization is most effective, but it has also non-negligible values in the rest of the discharge, because the production by Ar metastable–metastable ionization collisions is also important in the remaining part of the NG. The density profiles of the Ar_2^+ ions, on the other hand, are more spread out over the entire discharge region, because these species are produced mainly by Ar metastable–metastable and Hornbeck–Molnar associative ionization, and not by electron impact ionization. The electron

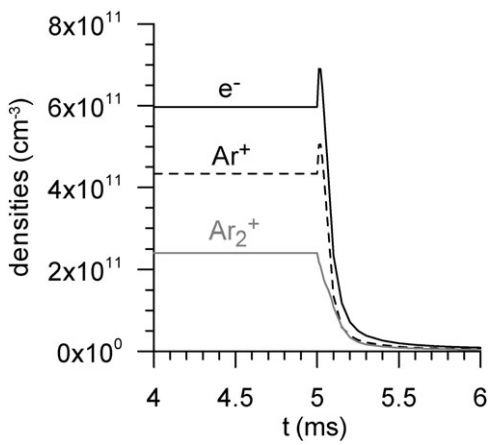

Fig. 4 Calculated electron, Ar^+ and Ar_2^+ ion densities at the maximum of their spatial profiles, as a function of time, at the end of the pulse and in the afterglow.

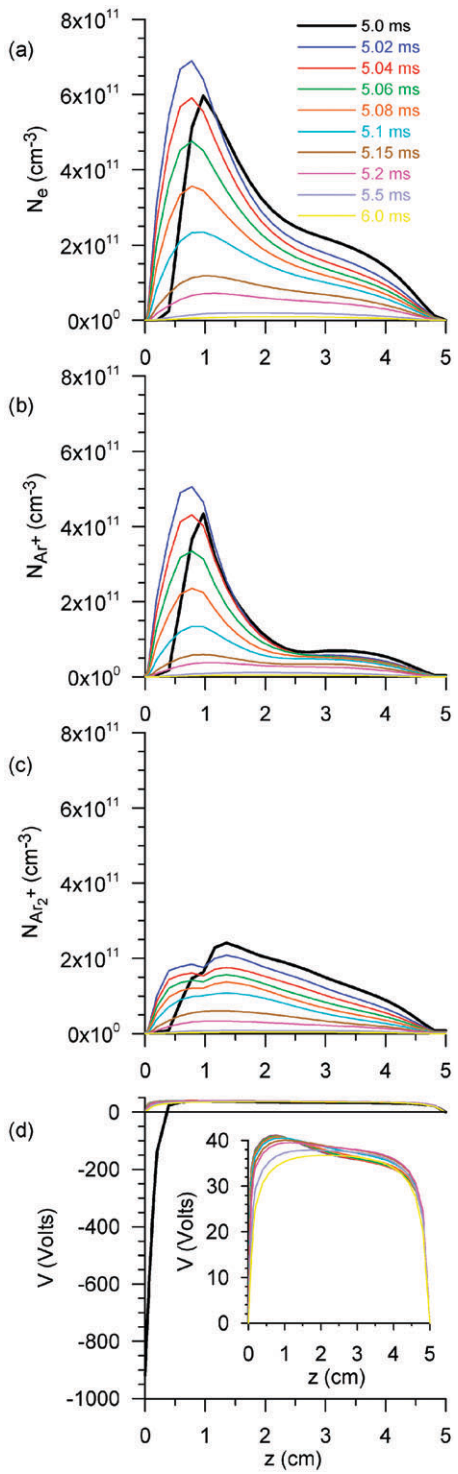

Fig. 5 Calculated one-dimensional spatial density profiles, obtained at the cell axis, of the electrons (a), Ar^+ ions (b), and Ar_2^+ ions (c), at different times, at the end of the pulse and in the afterglow. Also shown is the corresponding electric potential distribution at the cell axis, at the same times (d).

density in the NG is equal to the sum of Ar^+ and Ar_2^+ ion densities.

Upon pulse termination, the potential at the cathode drops to zero, and the values in the NG rise slightly to values of 35–40 V (see also inset in Fig. 5(d)). Note that this behaviour looks different from our previous results.[34] Indeed, in Fig. 2 of ref. 34, negative potentials were found in the CDS, even after pulse termination (up to 5.8 ms). The reason is that in our previous study, the applied voltage (*i.e.* the cathode potential) was assumed to drop slowly in the afterglow, to about zero at 6 ms. Hence, it is logical that the potential in the CDS then also drops slowly, as a result of this boundary condition. In the present calculations, however, the voltage (*i.e.*, cathode potential) was assumed to drop suddenly to zero after pulse termination, so there is no reason (or boundary condition) why the potential in the CDS should stay negative.

From the inset of Fig. 5(d) it is clear that shortly after pulse termination, the potential shows a broad maximum at the beginning of the NG and lower values in the second half of the NG, but it becomes more uniform at later times in the afterglow. As a result of this changing potential distribution upon pulse termination, the densities of electrons, Ar^+ and Ar_2^+ ions shift towards the cathode in the early afterglow, and the maximum electron and Ar^+ ion densities show an initial, minor rise immediately after pulse termination, before they drop to low values (*cf.* above). However, it should be noted that Rayleigh scattering experiments[35] revealed a small rise in the gas temperature near the cathode from about 550 K to 700 K upon pulse termination (see Fig. 3 of ref. 35). This yields a rise in diffusion coefficient, and thus an enhanced loss of electrons at the cell walls, which is not predicted by the model, because the temporal variation in gas temperature was not included. It is entirely possible that the latter effect compensates in reality for the small peak in the electron density in the early afterglow.

(b) Densities of Ar atoms in excited levels

Fig. 6 shows the population densities of Ar atoms in various excited levels, obtained at the maximum of their spatial profiles, as a function of time. The *n*-values correspond to the effective level numbers indicated in rectangular boxes in Fig. 2. The notations between brackets give information on the effective levels and their excitation energy. It is clear from Fig. 6(a) that the Ar metastable levels ($3p^5$ 4s; $n = 2$) have a longer lifetime in the negative glow than the other excited levels because they do not undergo radiative decay. For the lowest excited levels, up to the $3p^5$ 6p levels, with excitation energy around 15.0 eV, no rise in population density is calculated upon pulse termination (*cf.* Figs. 6 (b) and (c)). This suggests that these levels are not affected by electron–ion recombination. However, for the higher excited levels, with excitation energy of 15.2 eV and more, an afterpeak is predicted by the model, and the relative increase of this peak compared with the plateau value rises for higher excited levels, as can be seen by comparing Figs. 6 (d)–(h). The reason is that the highest excited levels, close to the ionization limit, are populated directly by electron–ion recombination (see Section 2 above), and they gradually decay by emission of radiation to the lower excited levels. Hence, the lower excited levels are only indirectly affected by electron–ion recombination, and the effect becomes of less importance for lower levels. This is at least in qualitative agreement with experimental

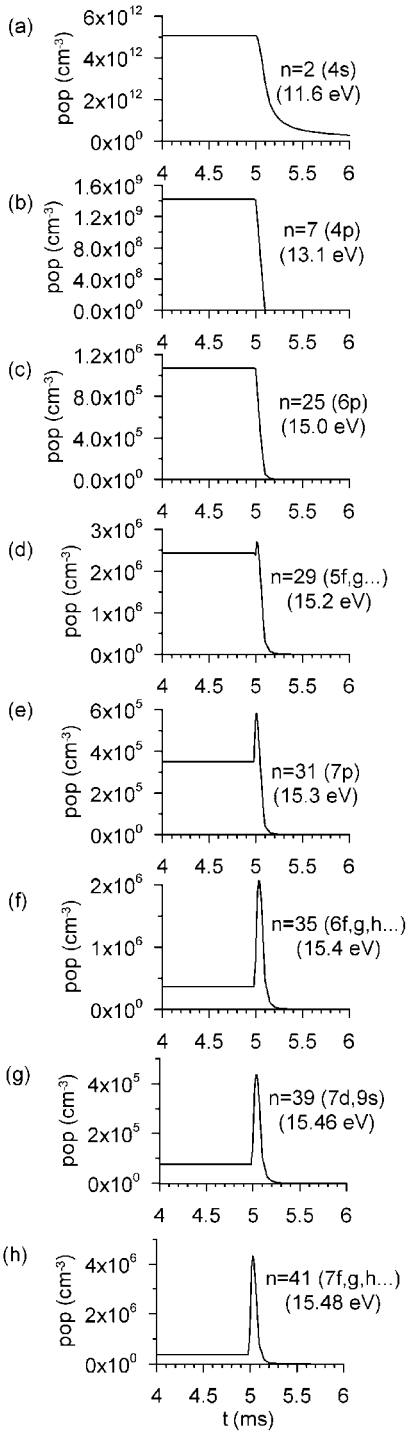

Fig. 6 Calculated level populations of several Ar excited levels, at the maximum of their spatial profiles, as a function of time, at the end of the pulse and in the afterglow. The *n*-values correspond to the effective level numbers, as defined in ref. 41 and illustrated in Fig. 2 above. The notations in brackets indicate the actual (effective) levels, as well as the excitation energy of the levels.

observations,[27,28,31] although the latter also exhibit a slight increase for lower excited levels.[30,31] Hence, the indication is that either electron–ion recombination, as the production process for the highest excited levels, or the Einstein transition probabilities for gradual radiative decay to lower levels, might be still underestimated in the model. Nevertheless, this is the first time that numerical simulations have, at least qualitatively, confirmed the hypothesis of electron–ion recombination followed by radiative decay as the responsible mechanism for the afterpeak behaviour in pulsed discharges.

In order to investigate which electron–ion recombination mechanism (*i.e.*, either three-body recombination or dissociative recombination) can account for this behaviour, we have to look in more detail to the rates of the various processes.

(c) Rates of ionization and recombination processes

Fig. 7(a) shows the rates of electron–Ar^+ ion three-body recombination (reaction 5 from Table 1) and electron–Ar_2^+ ion dissociative recombination (reaction 9 from Table 1), integrated over the entire glow discharge cell, as a function of time in the pulse and afterglow. For comparison, Fig. 7(b) illustrates the (spatially integrated) rates of electron impact ionization (reaction 1), Ar^+ ion impact ionization (reaction 2), fast Ar^0 atom impact ionization (reaction 3) and Ar metastable–metastable ionization (reaction 4), as production processes for the Ar^+ ions (and electrons), as well as the rates of Ar metastable–metastable associative ionization (reaction 7) and Hornbeck–Molnar associative ionization (reaction 8), as production mechanisms for the Ar_2^+ ions (and electrons), and finally also the rate of Ar^+ ion to Ar_2^+ ion conversion (reaction 6 from Table 1).

The total (*i.e.*, spatially integrated) rate of electron impact ionization is calculated to be 2.3×10^{17} s^{-1} during the pulse, but it drops almost instantaneously to zero upon pulse termination, as the electrons lose their energy by collisions and cannot be accelerated any more by the electric field, as soon as the applied voltage is switched off (*cf.* Fig. 3). The rates of fast Ar^+ ion and Ar^0 atom impact ionization were calculated to be about 3.5×10^{15} s^{-1} and 1.2×10^{16} s^{-1}, respectively, during the pulse and zero in the afterglow, and hence are of minor importance compared with electron impact ionization. Ar metastable–metastable ionization, on the other hand, is of the order of 5.6×10^{16} s^{-1} during most of the pulse, and hence contributes almost 20% to the formation of Ar^+ ions. Since the Ar metastable atoms decay rather slowly as a function of time upon pulse termination, the production of Ar^+ ions in the afterglow is entirely due to this process.

The formation of Ar_2^+ ions by Ar metastable–metastable associative ionization is almost equally important, with a calculated rate of 5.1×10^{16} s^{-1}, due to a slightly lower rate constant used (*cf.* Table 1). The rate of Hornbeck–Molnar associative ionization is only slightly lower ($\sim 4.5 \times 10^{16}$ s^{-1}), but it is characterized by a pronounced peak (up to 1.84×10^{17} s^{-1}) upon pulse termination, as a result of the enhanced level populations of the highly excited Ar levels in the early afterglow (see Fig. 6 above). This gives a supply of Ar_2^+ ions upon pulse termination, which are then available for electron–ion recombination in the afterglow (see below). Ar^+ to Ar_2^+ ion conversion was found to be of minor importance as the production mechanism for the Ar_2^+ ions, with a rate of the order of 10^{14} s^{-1}.

We are, however, especially interested in the loss of ions and electrons by electron–ion recombination, as this is generally believed[23–31] to be the responsible mechanism for the afterpeak formation in pulsed glow discharges. It is clear from Fig. 7(a) that dissociative recombination between Ar_2^+ ions and electrons is the dominant recombination mechanism. Its rate is about 5.7×10^{16} s^{-1} during the pulse, which rises to 2.2×10^{17} s^{-1} upon pulse termination. The rate of Ar^+ ion–electron three-body recombination is only of the order of 10^{11} s^{-1} during the pulse, and hence is negligible, but it jumps upon pulse termination up to values of about 7.4×10^{15} s^{-1}. This is attributed to the thermalization of the electrons in the afterglow, and the strong effect of this on the rate coefficient of three-body recombination (*cf.* the formula in Table 1, and Fig. 1 above). We have not explicitly calculated the electron thermalization process in our model, for the reasons explained

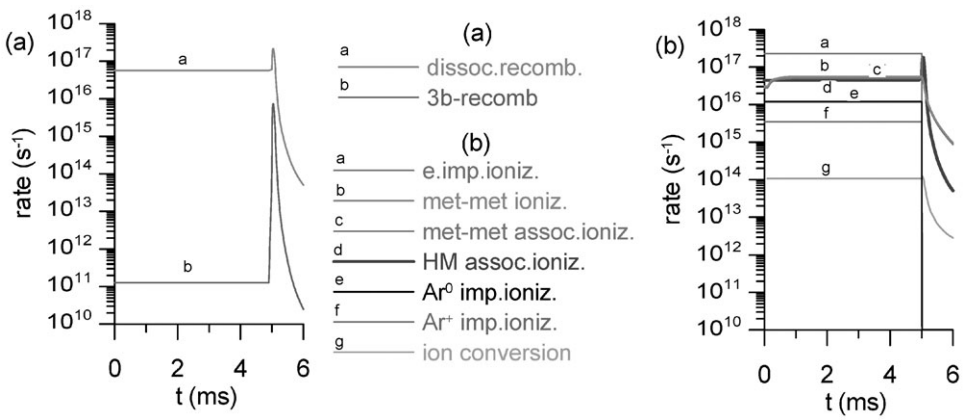

Fig. 7 Calculated rates of electron–ion three-body and dissociative recombination (a), as well as rates of electron, Ar^+ and fast Ar^0 impact ionization, Ar metastable–metastable ionization and associative ionization, Hornbeck-Molnar associative ionization, and Ar^+ to Ar_2^+ ion conversion (b), obtained by integration over the entire glow discharge cell, as a function of time, during and after the pulse.

in our previous paper,[34] but we have assumed that the electrons become thermalized during the first 100 μs of the afterglow, based on the observations by Biondi[48] and confirmed qualitatively by Li *et al.*[31] The dissociative recombination coefficient is not so strongly dependent on electron temperature (*cf.* again the formula in Table 1 and Fig. 1 above), hence the rise of the dissociative recombination rate upon pulse termination is less pronounced. Nevertheless, the rate of Ar_2^+–electron dissociative recombination in the afterglow is still several orders of magnitude higher than the rate of Ar^+–electron three-body recombination, as is apparent from Fig. 7(a).

(d) Effect of dissociative recombination in the afterpeak formation: model comparison with/without Ar_2^+ ions incorporated

Fig. 7 suggests that the Ar_2^+ ions are responsible for the afterpeak formation in pulsed glow discharges, due to dissociative recombination with electrons. To check this result, we have repeated the calculations without taking into account the Ar_2^+ ions in the model. Fig. 8 illustrates the results of this model, more specifically the temporal behaviour of the level populations for the same Ar excited levels as are depicted in Fig. 6 (again at the maximum of their spatial profiles). It is clear that the lowest levels (*e.g.*, $n = 2$, 7 and 25) exhibit the same temporal behaviour as in the model where Ar_2^+ ions were included (*cf.* Fig. 8 (a,b,c) with Fig. 6 (a,b,c)). This confirms our conclusion made above that these levels are not affected by dissociative recombination of Ar_2^+ ions, because the radiative decay from the higher levels seems not strong enough. The higher levels, such as $n = 29$, 31, 35 and 39, have the same density during the pulse as is found in the model with Ar_2^+ ions included, but upon pulse termination no afterpeak is observed. This clearly indicates that the afterpeak behaviour observed for these levels in Fig. 6 above can definitely be attributed to Ar_2^+–electron dissociative recombination. For still higher levels, an afterpeak was observed, even in the model where no Ar_2^+ ions were incorporated, as is shown for $n = 41$ in Fig. 8(h). This illustrates that Ar^+–electron three-body recombination plays a non-negligible role in the afterpeak formation mechanisms, but the effect is weaker than for dissociative recombination, and is only visible for the higher excited levels (such as $n = 41$ and above).

It is interesting to note out that, more than 60 years ago, a discrepancy was observed between theory and experiment on recombination rates in Ar discharge tubes.[49] Indeed, the experimentally observed recombination rate coefficient was much higher than predicted by theory. However, the theory had neglected dissociative recombination with Ar_2^+ ions, because molecular ions were assumed to be of minor importance in the discharge.[49] About 10 years later, Bates[50,51] and Biondi[52–55] pointed out that dissociative recombination with molecular ions is characterized by a much higher rate coefficient than recombination with atomic ions. Hence, it can be more important in rare gases, even when the molecular ions are less abundant than the atomic ions. These conclusions are nicely in line with our observations. In more recent work,[56,57] molecular ions (Ar_2^+ and He_2^+) and dissociative recombination are even expected to play a dominant role during the plasma decay phase of rare gas plasmas at atmospheric pressure. In ref. 58, a transition from electron–ion three-body recombination (occurring in the early afterglow) to dissociative recombination (in the later afterglow) was observed and qualitatively explained in an Ar afterglow plasma, in the pressure range of 5–18 Torr.

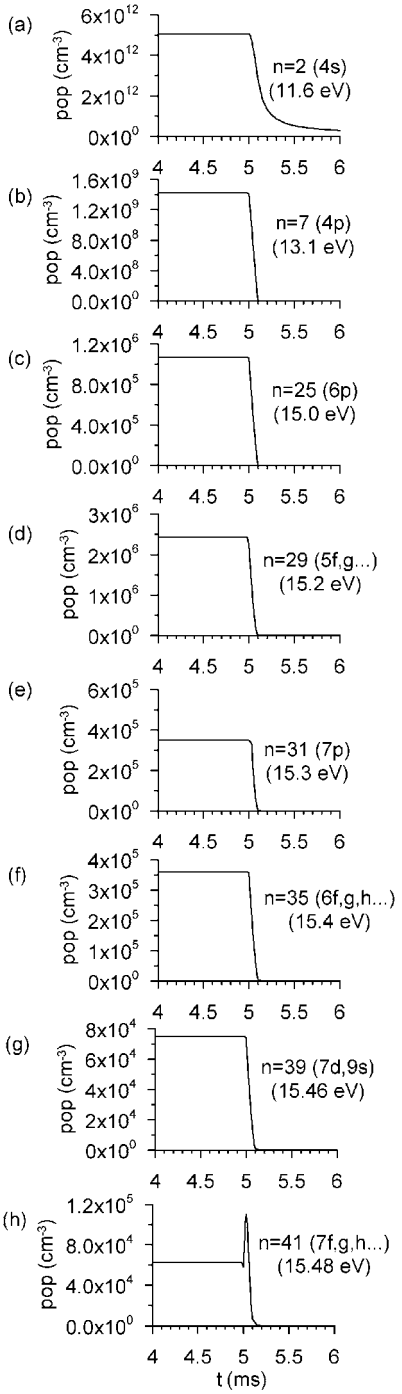

Fig. 8 Calculated level populations of the same Ar excited levels presented in Fig. 6, at the maximum of their spatial profiles, as a function of time, at the end of the pulse and in the afterglow, in the case when Ar_2^+ ions were not included in the model.

4. Discussion

From the above results, it is suggested that the following processes are taking place, during and after the pulse. The idea is schematically illustrated in Fig. 9. During the pulse, the glow discharge behaves as an ionizing plasma, with electron impact ionization as the dominant ionization mechanism, but Ar metastable–metastable ionization and associative ionization collisions, as well as Hornbeck–Molnar associative ionization, are also important processes in the formation of Ar^+ and Ar_2^+ ions. The latter process, *i.e.* Hornbeck–Molnar associative ionization, is counterbalanced by dissociative recombination between Ar_2^+ ions and electrons. Both mechanisms can be considered as forward and reverse processes of an equilibrium reaction (although strictly speaking the glow discharge is not in an equilibrium situation, so this is just a way of explaining the behaviour):

$$Ar^{**} + Ar^0 \underset{k_{DR}}{\overset{k_{HM}}{\rightleftarrows}} Ar_2^+ + e^-$$

Upon pulse termination, the electrons undergo thermalization, and hence the rate coefficient for dissociative recombination (k_{DR}) increases from roughly 1.6×10^{-7} cm^3 s^{-1} to 9×10^{-7} cm^3 s^{-1} (*cf.* Table 1 and Fig. 1), while the Hornbeck–Molnar associative ionization rate coefficient (k_{HM}) remains constant at 2×10^{-9} cm^3 s^{-1}. Hence, the equilibrium of the above reaction shifts to the left, resulting in higher Ar** excited level populations, and consequently in enhanced emission intensities in the afterglow. Because the highly excited Ar levels gradually decay to lower levels, also emission intensities originating from lower excited levels can exhibit a peak in the afterglow, but it will be less pronounced, as they are only indirectly affected by the recombination process. Besides Ar_2^+–electron dissociative recombination, Ar^+–electron three-body recombination also plays some role in the afterglow, but seems to affect only the highest excited levels.

This hypothesis sounds reasonable, but we still need to make a few comments. Experiments[27,28] indeed reveal that the enhancement in emission intensities is greatest for lines originating from the highest excited Ar levels, hence the recombination process must populate directly the highest excited Ar levels. This is generally true for recombination from Ar^+ ions,[43] as they represent the ionization limit (see Fig. 9). The Ar_2^+ ion (potential) energy, on the other hand, is only 14.43 eV (see above); hence dissociative recombination of ground state Ar_2^+ ions would probably populate Ar levels with an excitation energy around 14.43 eV, and not the highest excited levels. In fact, several authors[47,59–62] point out that dissociative recombination of ground state Ar_2^+ ions predominantly populates the 4p and 4p′ levels. Higher levels (such as 5p, 4d, 5d, 6s) can be populated, but at higher electron temperatures.[47] Therefore, in order to allow dissociative recombination to populate the highest excited levels, it is suggested that the Ar_2^+ ions do not only exist in the ground state, but mainly in vibrationally excited levels. The latter could be populated by Hornbeck–Molnar associative ionization of the highly excited Ar levels, as indicated in Fig. 9.

Biondi[43] states that the dissociative recombination rate dependence on the vibrational excitation in the molecular ion depends on the overlap between the initial ionic state and the intermediate state. It is therefore not possible to draw general conclusions, because the detailed curve crossings for a particular molecular system determine the variation.[43] In the case of argon, Shiu and Biondi[47] expect that the rate coefficient for dissociative recombination from vibrationally excited levels will be somewhat lower than from the ground state, but they do not say by how much the rate coefficients are lower. On the other hand, Cunningham *et al.*[63] measured a stronger (electron) temperature dependence for dissociative recombination of Ar_2^+ and Ne_2^+ ions in vibrationally excited states (with a temperature exponent of −1.5). This suggests that dissociative recombination involving vibrationally excited states will become relatively more important upon thermalization of the electrons in the afterglow.[63] It is also worth

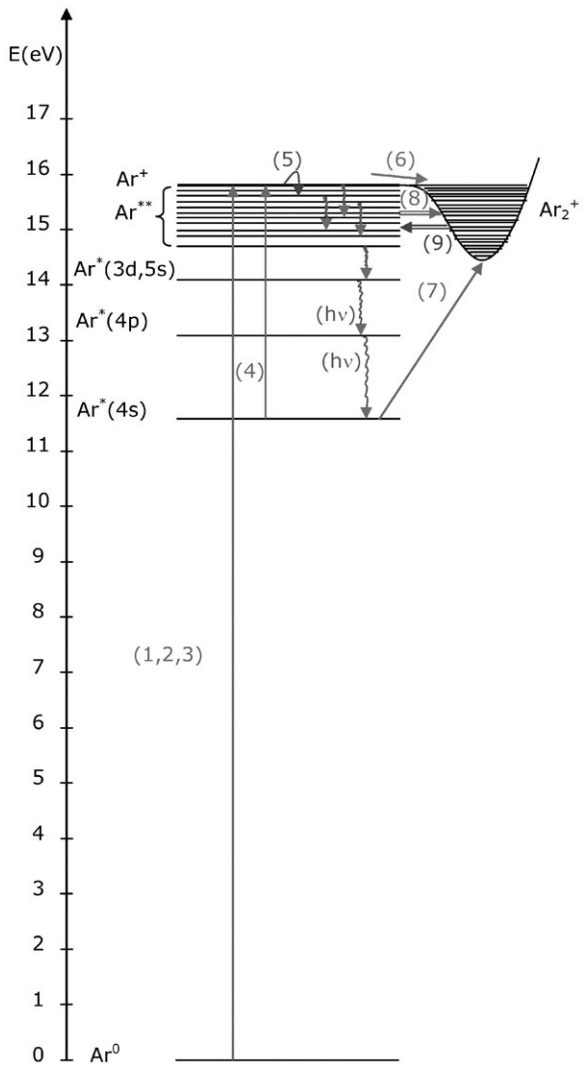

Fig. 9 Schematic picture of the relevant ionization, recombination and radiative processes playing a role in argon pulsed glow discharges. For clarity, different colours are used (in the HTML version) for the ionization processes (1, 2, 3, 4, 7 and 8, red), recombination (5 and 9, blue), conversion (down facing arrows other than 5, green) and radiative decay (6, purple). The numbers correspond to the reactions presented in Table 1.

mentioning that for the case of H_2, several authors[64–66] have reported that vibrationally excited H_2^+ ions give rise to the formation of highly excited H atoms by dissociative recombination. The dissociative recombination rate for these highly excited vibrational levels exceeds the rate for the lower vibrational levels by two orders of magnitude. Furthermore, it was reported that these vibrationally excited H_2^+ ions can be stable for a long time, before relaxing to lower levels.[64–66]

Rogers and Biondi[67] also concluded (in the case of helium) that it was necessary to postulate that the molecular ions are in vibrationally excited states as they undergo dissociative recombination in order to produce the high-lying atomic states, which yield the observed emission lines. The formation of these molecular ions in high-lying vibrational states is a reasonable consequence of the associative ionization reaction, in which the most likely binding collision is one in which a minimum loss of kinetic energy between two atoms takes place.[67] Furthermore, it was suggested that the probability of relaxation of the highly excited vibrational levels is very small ($<10^{-8}$), so that ions should persist in the higher vibrational states for a reasonably long time.[67] Finally, in the case of xenon, it was also reported that associative ionization yields the formation of Xe_2^+ ions in vibrationally excited levels, and that the latter gave rise to highly excited Xe levels as a result of dissociative recombination.[68]

In line with the conclusions of Rogers and Biondi,[67] we propose a similar mechanism: the forward reaction of Hornbeck–Molnar associative ionization (reaction 8 of Table 1) creates a large pool of Ar_2^+ ions in vibrationally excited levels, whereas the backward reaction of dissociative recombination (reaction 9), which becomes especially important in the afterglow due to the higher rate coefficient upon thermalization of the electrons, gives rise to the afterpeak formation in the level populations of highly excited Ar levels.

A second comment to be made is that the Ar_2^+ ions might be responsible for the afterpeak emissions of Ar lines, but experiments also reveal emission enhancements for the sputtered species.[26] If three-body recombination of atomic ions was not sufficiently important, the afterpeak would again need to be explained by dissociative recombination of molecular ions. Possible candidates could be dimers (M_2^+), but also argides (MAr^+), hydrides (MH^+) or other clusters. Because recombination rate constants for such species are not directly available, this hypothesis cannot yet be checked with model calculations.

Finally, experimental observations also indicate some rise in Ar metastable densities[27,30,31] (and consequently in analyte ion intensities,[23–26,31] due to enhanced Penning ionization), but this does not yet follow from our model calculations, either because the rate coefficients for electron–ion recombination or the Einstein transition probabilities for radiative decay are still underestimated in the model, or because another process is still lacking in the model. For instance, it is argued by Mason *et al.*[69] that a large fraction of excited states could exist in auto-ionizing levels, *i.e.*, above the ionization potential of neutral Ar, and these states might radiatively decay in the afterglow. These levels normally arise from the excitation of a second electron or an inner electron. However, whilst in some cases such levels are stable because selection rules prevent mixing with the ionization continuum, in most cases configuration interaction occurs, and the excited state ionizes very rapidly. Such auto-ionizing levels have lifetimes as short as 10^{-13} s (compared with the normal radiative lifetimes of 10^{-9} s) and are therefore unlikely to play any role in the afterglow. In practice, transitions from such levels can only be observed in absorption, and then they have extremely large line-widths, corresponding to their short lifetime (see, for example, ref. 70).

It is also quite possible that the physics taking place is still more complicated. For instance, recent experiments[71] on pulsed low pressure (5–9 Pa) discharges have revealed that the mean electron energy in the late afterglow exhibits high constant values. This indicates that energy losses of the electrons need to be compensated for by some electron re-heating mechanism. The spatio-temporal dynamics of the discharge were therefore examined with modelling. It was demonstrated that re-heating of the electrons is possible by superelastic collisions from the upper to the lower metastable level, and by chemo-ionization involving the metastable levels.[71] These processes apply, of course, to another discharge regime (the low pressure inductively coupled plasma), but it shows that the reality can be still more complicated than the currently accepted theories.

5. Conclusion

The aim of this paper was to investigate which mechanisms of electron–ion recombination can solve the mystery of afterpeak formation in pulsed glow discharges. Our study strongly suggests that dissociative recombination between Ar_2^+ ions and electrons is mainly responsible for this afterpeak formation. Ar^+–electron three-body recombination also plays a non-negligible role, but seems to manifest itself only in the highest excited levels.

Certainly, our model is not yet perfect, but already it can shed more light on the processes responsible for afterpeak formation in the afterglow. To further optimize our understanding of these processes, experimental studies will be needed, *e.g.*, on the densities of Ar_2^+ ions, and if possible the partition function over various vibrationally excited levels, as well as on other cluster ions associated with the sputtered species.

Acknowledgements

The author thanks G. Gamez, G. Jackson, G. Hieftje and R. Gijbels for the interesting discussions and comments on the paper, and E. Steers for supplying information on auto-ionizing states.

References

1 W. W. Harrison, W. Hang, X. Yan, K. Ingeneri and C. Shilling, *J. Anal. At. Spectrom.*, 1997, **12**, 891.
2 W. W. Harrison, *J. Anal. At. Spectrom.*, 1998, **13**, 1051.
3 W. W. Harrison, C. Yang and E. Oxley, *Anal. Chem.*, 2001, **73**, 480A.
4 X. Yan, W. Hang, B. W. Smith, J. D. Winefordner and W. W. Harrison, *J. Anal. At. Spectrom.*, 1998, **13**, 1033.
5 C. Yang and W. W. Harrison, *Spectrochim. Acta, Part B*, 2001, **56**, 1195.

6 X. Yan, K. Ingeneri, W. Hang and W. W. Harrison, *J. Anal. At. Spectrom.*, 2001, **16**, 819.
7 S. Potapov, E. Izrailov, V. Vergizova, M. Voronov, S. Suprunovich, M. Slyadnev and A. Ganeev, *J. Anal. At. Spectrom.*, 2003, **18**, 564.
8 C. Yang, K. Ingeneri and W. W. Harrison, *J. Anal. At. Spectrom.*, 1999, **14**, 693.
9 E. Oxley, C. Yang and W. W. Harrison, *J. Anal. At. Spectrom.*, 2000, **15**, 1241.
10 R. E. Steiner, C. L. Lewis and V. Majidi, *J. Anal. At. Spectrom.*, 1999, **14**, 1537.
11 V. Majidi, M. Moser, C. Lewis, W. Hang and F. L. King, *J. Anal. At. Spectrom.*, 2000, **15**, 19.
12 C. L. Lewis, M. A. Moser, W. Hang, D. E. Dale, Jr, D. C. Hassell and V. Majidi, *J. Anal. At. Spectrom.*, 2003, **18**, 629.
13 L. Li, C. M. Barshick, J. T. Millay, A. V. Welty and F. L. King, *Anal. Chem.*, 2003, **75**, 3953.
14 C. L. Lewis, M. A. Moser, D. E. Dale, Jr, W. Hang, D. Hassell and V. Majidi, *Anal. Chem.*, 2003, **75**, 1983.
15 L. Li, J. T. Millay, J. P. Turner and F. L. King, *J. Am. Soc. Mass Spectrom.*, 2004, **15**, 87.
16 W. Hang, C. Baker, B. W. Smith, J. D. Winefordner and W. W. Harrison, *J. Anal. At. Spectrom.*, 1997, **12**, 143.
17 D. C. Duckworth, D. H. Smith and S. A. McLuckey, *J. Anal. At. Spectrom.*, 1997, **12**, 43.
18 C. Yang, M. Mohill and W. W. Harrison, *J. Anal. At. Spectrom.*, 2000, **15**, 1255.
19 A. Bengtson, C. Yangan and W. W. Harrison, *J. Anal. At. Spectrom.*, 2000, **15**, 1279.
20 Y. Su, Z. Zhou, P. Yang, X. Wang and B. Huang, *Spectrochim. Acta, Part B*, 1997, **52**, 633.
21 J. H. Barnes IV, O. A. Gron and G. M. Hieftje, *J. Anal. At. Spectrom.*, 2004, **19**, 1564.
22 J. Pisonero, K. Turney, N. Bordel, A. Sanz-Medel and W. W. Harrison, *J. Anal. At. Spectrom.*, 2003, **18**, 624.
23 F. L. King and C. Pan, *Anal. Chem.*, 1993, **65**, 735.
24 J. A. Klingler, C. M. Barshick and W. W. Harrison, *Anal. Chem.*, 1991, **63**, 2571.
25 J. A. Klingler, P. J. Savickas and W. W. Harrison, *J. Am. Soc. Mass Spectrom.*, 1990, **1**, 138.
26 C. L. Lewis, G. P. Jackson, S. K. Doorn, V. Majidi and F. L. King, *Spectrochim. Acta, Part B*, 2001, **56**, 487.
27 G. P. Jackson, C. L. Lewis, S. K. Doorn, V. Majidi and F. L. King, *Spectrochim. Acta, Part B*, 2001, **56**, 2449.
28 G. P. Jackson and F. L. King, *Spectrochim. Acta, Part B*, 2003, **58**, 1417.
29 G. P. Jackson and F. L. King, *Spectrochim. Acta, Part B*, 2003, **58**, 185.
30 C. L. Lewis, L. Li, J. T. Millay, S. Downey, J. Warrick and F. L. King, *J. Anal. At. Spectrom.*, 2003, **18**, 527.
31 L. Li, J. Robertson-Honecker, V. Vaghela and F. L. King, *Spectrochim. Acta, Part B*, 2006, **61**, 722.
32 A. Bogaerts and R. Gijbels, *J. Anal. At. Spectrom.*, 2000, **15**, 895.
33 A. Bogaerts and R. Gijbels, *J. Anal. At. Spectrom.*, 2001, **16**, 239.
34 A. Bogaerts, R. Gijbels and G. P. Jackson, *J. Anal. At. Spectrom.*, 2003, **18**, 533.
35 G. Gamez, A. Bogaerts and G. M. Hieftje, *J. Anal. At. Spectrom.*, 2006, **21**, 350.
36 A. Bogaerts and R. Gijbels, *J. Appl. Phys.*, 1996, **79**, 1279.
37 A. Bogaerts, M. van Straaten and R. Gijbels, *Spectrochim. Acta, Part B*, 1995, **50**, 179.
38 A. Bogaerts, R. Gijbels and W. J. Goedheer, *J. Appl. Phys.*, 1995, **78**, 2233.
39 A. Bogaerts and R. Gijbels, *J. Appl. Phys.*, 1999, **86**, 4124.
40 A. Bogaerts and R. Gijbels, *J. Appl. Phys.*, 1995, **78**, 6427.
41 A. Bogaerts, R. Gijbels and J. Vlcek, *J. Appl. Phys.*, 1998, **84**, 121.
42 N. B. Kolokolov and A. G. Blagoev, *Phys.–Usp.*, 1993, **36**, 152.
43 M. A. Biondi, in *Applied Atomic Collision Physics. Vol. 3: Gas Lasers*, eds. E. W. McDaniel and W. L. Nighan, Academic Press, New York, 1982, ch. 6.
44 R. Johnsen, A. Chen and M. A. Biondi, *J. Chem. Phys.*, 1980, **73**, 1717.
45 P. M. Becker and F. W. Lampe, *J. Chem. Phys.*, 1965, **42**, 3857.
46 F. J. Mehr and M. A. Biondi, *Phys. Rev.*, 1968, **176**, 322.
47 Y.-J. Shiu and M. A. Biondi, *Phys. Rev. A: At., Mol., Opt. Phys.*, 1978, **17**, 868.
48 M. A. Biondi, *Phys. Rev.*, 1952, **88**, 660.
49 D. R. Bates, R. A. Buckingham, H. S. W. Massey and J. J. Unwin, *Proc. R. Soc. London, Ser. A*, 1931, **A176**, 322.
50 D. R. Bates, *Phys. Rev.*, 1950, **77**, 718.
51 D. R. Bates, *Phys. Rev.*, 1950, **78**, 492.
52 M. A. Biondi and S. C. Brown, *Phys. Rev.*, 1949, **76**, 1697.
53 M. A. Biondi, *Phys. Rev.*, 1951, **83**, 1078.
54 M. A. Biondi and T. Holstein, *Phys. Rev.*, 1951, **82**, 962.
55 M. A. Biondi, *Phys. Rev.*, 1963, **129**, 1181.
56 M. J. vande Sande, P. van Eck, A. Sola, A. Gamero and J. J. A. M. van der Mullen, *Spectrochim. Acta, Part B*, 2003, **58**, 783.
57 J. Jonkers, M. J. van de Sande, A. Sola, A. Gamero, A. Rodero and J. J. A. M. van der Mullen, *Plasma Sources Sci. Technol.*, 2003, **12**, 464.
58 A. Funahashi, T. Makihira and S. Takeda, *J. Phys. Soc. Jpn*, 1970, **29**, 441.
59 M. Guna, L. Simons, K. Hardy and J. Peterson, *Phys. Rev. A: At., Mol., Opt. Phys.*, 1999, **60**, 306.
60 T. Okada and M. Sugarawa, *Jpn J. Appl. Phys., Part 1*, 1995, **34**, 5829.
61 G. E. Veatch and H. J. Oskam, *Phys. Rev.*, 1970, **1**, 1498.
62 L. Frommhold and M. A. Biondi, *Phys. Rev.*, 1969, **185**, 244.
63 A. J. Cunningham and R. M. Hobson, *Phys. Rev.*, 1969, **185**, 98.
64 W. J. van der Zande, J. Semaniak, V. Zengin, G. Sundström, S. Rosén, C. Strömholm, S. Datz, H. Danared and M. Larsson, *Phys. Rev. A: At., Mol., Opt. Phys.*, 1996, **54**, 5010.
65 M. I. Chibisov, J. B. A. Mitchell, P. J. T. Van der Donk, F. B. Yousif and T. J. Morgan, *Phys. Rev. A: At., Mol., Opt. Phys.*, 1997, **56**, 443.
66 J. B. A. Mitchell, F. B. Yousif, P. J. T. Van der Donk, T. J. Morgan and M. I. Chibisov, *Int. J. Mass Spectrom. Ion Processes*, 1995, **149/150**, 153.
67 W. A. Rogers and M. A. Biondi, *Phys. Rev.*, 1964, **134**, A1215.
68 X. K. Hu, J. B. A. Mitchell and R. H. Lipson, *Phys. Rev. A: At., Mol., Opt. Phys.*, 2000, **62**, 052712.
69 R. S. Mason, P. D. Miller and I. P. Mortimer, *Phys. Rev. E: Stat. Phys., Plasmas, Fluids, Relat. Interdiscip. Top.*, 1997, **55**, 7462.
70 A. Thorne, *Spectrophysics*, Chapman and Hall, 1974, pp. 56–60.
71 G. Wenig, M. Schulze, P. Awakowicz and A. v. Koedell, *Plasma Sources Sci. Technol.*, 2006, **15**, S35.

